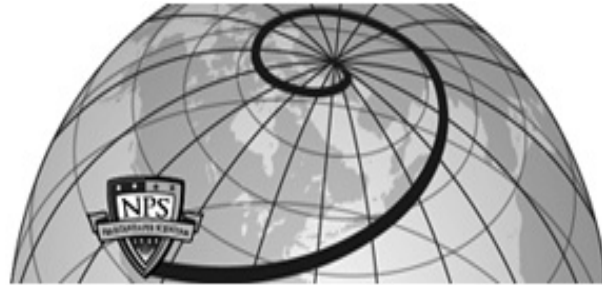




Institutional Archive of the Naval Postgraduate School



## Calhoun: The NPS Institutional Archive

---

Faculty and Researcher Publications

Faculty and Researcher Publications

---

2012

# Equilibrium transport in double-diffusive convection

Radko, Timour

---

<http://hdl.handle.net/10945/42122>



<http://www.nps.edu/library>

Calhoun is a project of the Dudley Knox Library at NPS, furthering the precepts and goals of open government and government transparency. All information contained herein has been approved for release by the NPS Public Affairs Officer.

Dudley Knox Library / Naval Postgraduate School  
411 Dyer Road / 1 University Circle  
Monterey, California USA 93943

# Equilibrium transport in double-diffusive convection

Timour Radko<sup>†</sup> and D. Paul Smith

Department of Oceanography, Naval Postgraduate School, Monterey, CA 93943, USA

(Received 18 March 2011; revised 2 August 2011; accepted 7 August 2011;  
first published online 28 September 2011)

A theoretical model for the equilibrium double-diffusive transport is presented which emphasizes the role of secondary instabilities of salt fingers in saturation of their linear growth. Theory assumes that the fully developed equilibrium state is characterized by the comparable growth rates of primary and secondary instabilities. This assumption makes it possible to formulate an efficient algorithm for computing diffusivities of heat and salt as a function of the background property gradients and molecular parameters. The model predicts that the double-diffusive transport of heat and salt rapidly intensifies with decreasing density ratio. Fluxes are less sensitive to molecular characteristics, mildly increasing with Prandtl number ( $Pr$ ) and decreasing with diffusivity ratio ( $\tau$ ). Theory is successfully tested by a series of direct numerical simulations which span a wide range of  $Pr$  and  $\tau$ .

**Key words:** double diffusive convection, instability, ocean processes

## 1. Introduction

Double-diffusion is the instability of a stratified fluid at rest whose density is determined by two components diffusing at different rates. Stern (1960) demonstrated that such a configuration can be unstable even if the density of the fluid is increasing downwards. The resulting double-diffusive convection has long been recognized as a significant, and in many cases dominant, mixing process in the ocean, where warm and salty water is often located above cold and fresh. In this case, the faster diffuser (temperature  $T$ ) is stabilizing and the slower diffuser (salinity  $S$ ) is destabilizing, resulting in the salt finger form of double-diffusive convection, which is the main focus of our discussion. In addition to oceanographic applications, the compositionally driven double-diffusive convection affects the heat and material transport in a variety of other geophysical and astrophysical fluid systems, from magmatic melts (Tait & Jaupart 1989) to the interiors of giant planets and stars (Guillot 1999; Vauclair 2004; Charbonnel & Zahn 2007; Stancliffe *et al.* 2007).

A fundamental question in double-diffusive convection theory concerns the equilibrium transport of temperature, salinity, chemical tracers, and momentum. The quantification of double-diffusive fluxes and their dependence on the background temperature and salinity gradients – so-called flux-gradient laws – is an essential step in linking the microstructure dynamics with larger scales of motion. This problem

<sup>†</sup>Email address for correspondence: tradko@nps.edu

has motivated numerous laboratory (e.g. Lambert & Demenkow 1972; Griffiths & Ruddick 1980) and field (Schmitt *et al.* 1987, 2005) experiments, as well as theoretical (Stern 1969; Kunze 1987) and numerical (Shen 1995; Stern, Radko & Simeonov 2001; Kimura & Smyth 2007, 2011; Traxler *et al.* 2011; Stellmach *et al.* 2011) models. While the linear stability theory of double-diffusion (Stern 1960; Baines & Gill 1969) is well developed and fully understood, it does not explain the saturation of primary double-diffusive instabilities. The problem of equilibrium double-diffusive transport is complicated and principally nonlinear.

Numerous attempts have been made to deduce flux-gradient laws from first principles. The first and perhaps most influential idea was introduced by Stern (1969), who suggested that the linear growth of salt fingers is arrested when the Stern number

$$A = \frac{\alpha F_{T\text{dim}} - \beta F_{S\text{dim}}}{\nu(\alpha \bar{T}_z - \beta \bar{S}_z)} \quad (1.1)$$

reaches  $O(1)$ .  $F_{T\text{dim}}$  and  $F_{S\text{dim}}$  here are the temperature and salinity fluxes;  $\bar{T}_z$  and  $\bar{S}_z$  are the vertical gradients;  $\alpha$ ,  $\beta$  are the thermal expansion and haline contraction coefficients respectively;  $\nu$  is the molecular viscosity. Stern's physical argument is compelling. When  $A$  exceeds unity, the unbounded salt finger system becomes unstable with respect to collective instability, a term used to describe the spontaneous excitation of gravity waves by salt fingers. Stern suggested that collective instability could disrupt salt fingers, thereby arresting the development of primary instabilities.

At first glance, various pieces of indirect evidence seem to validate Stern's hypothesis. For instance, oceanographic measurements (Hebert 1988; Inoue *et al.* 2008) tend to produce  $O(1)$  values of  $A$ . Additionally, Kunze (1987) gave an alternative argument in support of the Stern number constraint. He showed that the Stern number of unity is equivalent to the Richardson number ( $Ri$ ) of  $1/4$  based on scales of individual salt fingers. Kunze suggested that the well-known criterion for the instability of horizontal, inviscid and non-diffusive parallel flows (Richardson 1920; Howard 1961; Miles 1961), i.e.  $Ri < 1/4$ , can be extended to viscous, diffusive and vertically oriented fingers.

However, closer inspection has revealed certain inconsistencies in the Stern–Kunze hypothesis. For instance, in many laboratory experiments, salt and sugar replace heat and salt as buoyancy components (e.g. Stern & Turner 1969; Lambert & Demenkow 1972; Griffiths & Ruddick 1980; Taylor & Veronis 1996; Krishnamurti 2003). Typical values of Stern number in this case can be extremely low. Lambert & Demenkow (1972) report Stern numbers as low as  $A = 2 \times 10^{-3}$ , casting some doubt on the generality of the Stern number constraint. On the theoretical side, a critical advance was made by Holyer (1984), who performed a formal linear stability analysis for vertical steady salt fingers. She discovered direct, relatively small-scale – comparable to the salt finger width – secondary instabilities, which typically grow much faster than the collective instability modes. Unlike collective instabilities, Holyer modes grow regardless of the (finite) amplitude of salt fingers and thus regardless of the specific values of  $A$ . Numerical simulations (Shen 1995; Radko & Stern 1999) confirmed Holyer's ideas by demonstrating that the equilibration of salt fingers occurs by means of the nonlinear interaction of primary instabilities with Holyer modes. Furthermore, the eddy diffusivities of heat and salt from simulations (e.g. Stern *et al.* 2001) and available observations (St Laurent & Schmitt 1999) monotonically decrease with the density ratio, whereas the opposite trend was expected based on the Stern–Kunze constraint. Two-dimensional numerical experiments in Whitfield *et al.* (1989) with

various molecular parameters resulted in Stern numbers that varied by a factor of 3400. The most recent three-dimensional simulations of the heat–salt system (Traxler *et al.* 2011) indicate that, as the density ratio ( $R_\rho = \alpha\bar{T}_z/\beta\bar{S}_z$ ) increases from 1.2 to 10, the Stern number in the equilibrium flow reduces by more than two orders of magnitude, from  $A = 76$  to  $A = 0.6$ .

Concerns with regard to the Stern number constraint have motivated the development of alternative models. While the general analytical description of the equilibrium double-diffusive transport is still lacking, several cases have already been successfully treated. Weakly nonlinear instability theory describes salt finger patterns, dynamics, and transport characteristics for the parameters near the point of marginal instability (Proctor & Holyer 1986; Radko & Stern 1999, 2000; Stern & Simeonov 2004; Radko 2010). Promising attempts to formulate physically based parametrizations of salt finger transport include the mixing length model (Stern & Simeonov 2005), a double-diffusive version of the upper bound theory (Balmforth *et al.* 2006), a second-order closure approach (Canuto, Cheng & Howard 2008), and various phenomenological models (Shen 1995; Merryfield & Grinder 1999; Radko 2008). In this paper, we propose what appears to be, to date, the most general algorithm for estimating the equilibrium salt finger transport. The model is based on the properties of secondary salt finger instabilities and can be applied to a variety of parameter regimes, including small, moderate, and large Prandtl numbers, and a wide range of diffusivity ratios.

Our story is a new variation on an old theme – a theme that appears, explicitly or implicitly, in almost all theories of equilibrium double-diffusive convection (e.g. Stern 1969; Holyer 1984; Kunze 1987; Stern & Simeonov 2005; Radko 2010). We revisit the idea of a competition between linear mechanisms involved in the growth of salt fingers and the disruptive action of their secondary instabilities. At the same time, we strive to avoid some debatable assumptions of earlier models, such as the link between secondary instabilities and Stern number. The competition between primary and secondary instabilities is concisely phrased in the growth rate balance assumption

$$\lambda_2 = C\lambda_1, \quad (1.2)$$

where  $\lambda_1$  is the typical growth rate of linear salt fingers,  $\lambda_2$  is the growth rate of their secondary instabilities, and  $C$  is a dimensionless order-one quantity that can be calibrated on the basis of simulations or experiments. The primary growth rate  $\lambda_1$  is determined by the background gradients of temperature and salinity and by molecular characteristics (diffusivities and viscosity). The secondary instability  $\lambda_2$  is also affected by these quantities, but, additionally, it depends very strongly on the amplitude of primary salt fingers. Thus, for any given background parameters and a value of  $C$ , the growth rate balance (1.2) implicitly determines the equilibrium amplitude of salt fingers.

The physical reasoning behind (1.2) is straightforward. As initially weak salt fingers, emerging from random small scale perturbations, grow in time, they start to develop secondary instabilities (Holyer 1984). Unlike the primary ones, the growth rate of secondary instabilities monotonically increases with the amplitude of fingers. At first, the growth of secondary instabilities is too slow to inflict any significant damage on growing primary modes – the evolution of small amplitude fingers is adequately captured by the linear theory. However, at some point, the growth rate of secondary instabilities exceeds the primary growth rates. As a result, the secondary instabilities start to gain in magnitude, rapidly reaching the level of primary modes.

Their interaction nonlinearly suppresses the growth of salt fingers. At this stage, the system reaches statistical equilibrium.

In this study, condition (1.2) is used as the basis for an algorithm to determine the equilibrium amplitude of salt fingers. The growth of primary modes ( $\lambda_1$ ) is evaluated from the linear instability theory (Stern 1960; Baines & Gill 1969). For any given amplitude of salt fingers, the growth rate of secondary instabilities ( $\lambda_2$ ) can be computed using elements of Floquet theory as in Holyer (1984). The amplitude of fingers is iteratively adjusted until  $\lambda_1$  and  $\lambda_2$  satisfy the growth rate balance (1.2). The model predictions are then conveniently expressed in terms of the equilibrium eddy fluxes of heat and salt.

This paper is organized as follows. In § 2, we present preliminary direct numerical simulations (DNS), focusing our inquiry on the equilibration of primary instability. A theoretical model of equilibration is presented in § 3. We compute the temperature and salinity fluxes as a function of density ratio for the oceanographic case ( $Pr = 7, \tau = 0.01$ ) and successfully test (§ 4) the theoretical prediction by DNS. In § 5, we explore a broader parameter range, including the low-Prandtl-number regime, relevant for astrophysical applications, and high Prandtl numbers, relevant for magmatic melts. Each case is compared with the corresponding DNS. We summarize and draw conclusions in § 6.

## 2. Preliminary calculations

Following Radko & Stern (1999), we separate the temperature and salinity fields into the basic state  $(\bar{T}, \bar{S})$ , representing a uniform vertical gradient, and a departure  $(T, S)$  from it. The Boussinesq equations of motion are expressed in terms of  $T, S$  and non-dimensionalized using  $l = (k_T v / g \alpha \bar{T}_z)^{1/4}$ ,  $k_T/l$ ,  $l^2/k_T$ , and  $\rho_0 v k_T / l^2$  as the scales of length, velocity, time and pressure respectively. Here,  $(k_T, k_S)$  denote the molecular diffusivities of heat and salt and  $\rho_0$  is the reference density used in the Boussinesq approximation. The expansion/contraction coefficients are incorporated in  $(T, S)$ , and  $\alpha \bar{T}_z l$  is used as the scale for both temperature and salinity perturbations, resulting in

$$\left. \begin{aligned} \frac{\partial T}{\partial t} + \mathbf{v} \cdot \nabla T + w &= \nabla^2 T, \\ \frac{\partial S}{\partial t} + \mathbf{v} \cdot \nabla S + \frac{w}{R_\rho} &= \tau \nabla^2 S, \\ \frac{1}{Pr} \left( \frac{\partial}{\partial t} \mathbf{v} + \mathbf{v} \cdot \nabla \mathbf{v} \right) &= -\nabla p + (T - S)\mathbf{k} + \nabla^2 \mathbf{v}, \\ \nabla \cdot \mathbf{v} &= 0, \end{aligned} \right\} \quad (2.1)$$

where  $\mathbf{v} = (u, v, w)$  is the velocity vector and  $\mathbf{k}$  is the vertical unit vector. This system is unstable with respect to salt fingering (Stern 1960) for

$$1 < R_\rho < 1/\tau. \quad (2.2)$$

The key non-dimensional numbers governing the evolution of system (2.1) are the Prandtl number  $Pr = v/k_T$ , the diffusivity ratio  $\tau = k_S/k_T$ , and the background density ratio  $R_\rho = \alpha \bar{T}_z / \beta \bar{S}_z$ . We also assume that, for given  $T$ - $S$  gradients, fluxes are independent of the non-dimensional parameters related to the domain size, such as the Rayleigh number – an assumption that has been validated in previous studies (e.g. Radko & Stern 1999).

To gain a preliminary understanding of the mechanics of equilibration ( $R_\rho, Pr, \tau$ ), the equations in (2.1) were solved numerically. We assume triply periodic boundary conditions for  $T$ ,  $S$ ,  $p$ , and  $\mathbf{v}$ , and integrate the governing equations using a dealiased pseudospectral method described in Radko & Stern (1999). In the following calculation, we use parameters relevant in the oceanographic (heat/salt) context:  $\tau = 0.01$  and  $Pr = 7$ . The overall density ratio is  $R_\rho = 1.9$ , which is representative of the main Atlantic thermocline. The size of the computational domain ( $L_x = 38.2, L_y = 38.2, L_z = 76.3$ ) is equivalent to  $(5 \times 5 \times 10)$  linearly fastest-growing finger wavelengths ( $d$ ). The flow was resolved by a uniform mesh with  $(N_x \times N_y \times N_z) = (256 \times 256 \times 512)$  elements, and the model was initialized from rest by a small-amplitude random computer-generated initial  $(T, S)$  distribution. After a few characteristic growth periods, active statistically steady double-diffusive convection was established. Figure 1(a) shows a typical instantaneous ( $t = 20$ ) temperature field in the initial stage of linear growth. As expected from the linear stability theory, the most rapidly growing perturbations take the form of the vertically uniform salt fingers. Such structures are known as elevator modes – a term that will be used throughout this study to distinguish vertical fingers from irregular patterns realized at the fully nonlinear stage of development. Figure 1(b) presents the fully developed equilibrium regime ( $t = 50$ ). While the previously dominant elevator mode is still visible, it is now comparable in magnitude to the secondary instabilities, which act to distort the vertical fingers, adversely affecting their growth. This stage is characterized by the irregular transient patterns in the temperature field, which is a consequence of the nonlinear interaction between the elevator modes and their secondary instabilities.

The transition to the statistically steady regime is illustrated in figure 2, which shows the evolution of the spatially averaged downward temperature and salinity fluxes  $(F_T, F_S) = (-\bar{w}T, -\bar{w}S)$ ; the sign convention is dictated by considerations of convenience. Note that the heat flux in our system of non-dimensionalization is  $F_T = Nu - 1$ , where  $Nu$  is the Nusselt number – the ratio of the total heat flux to the (much weaker) molecular diffusive flux. The initial stage of the simulation ( $t < 30$ ) is characterized by the exponential growth of fluxes, which is followed by their equilibration. After equilibration, the intensity of salt fingering remains statistically steady.

The non-dimensional fluxes  $(F_T, F_S)$  can be converted to the dimensional eddy diffusivities of heat and salt ( $K_{Tdim}, K_{Sdim}$ ) using

$$K_{Tdim} = F_T k_T, \quad K_{Sdim} = F_S k_T R_\rho. \quad (2.3)$$

The time mean  $T$ - $S$  fluxes, averaged over the second half of the experiment in figure 2, are  $F_T = 40.88, F_S = 75.88$ , which corresponds to the dimensional diffusivities of heat and salt of

$$K_{Tdim} = 5.6 \times 10^{-6} \text{ m}^2 \text{ s}^{-1}, \quad K_{Sdim} = 2.0 \times 10^{-5} \text{ m}^2 \text{ s}^{-1}. \quad (2.4)$$

These values are comparable to the observational estimates (St Laurent & Schmitt 1999). Prediction (2.4) is also broadly consistent with earlier simulations in Stern *et al.* (2001), who finds, for the density ratio of  $R_\rho = 2$ ,  $K_{Tdim} = 7.6 \times 10^{-6} \text{ m}^2 \text{ s}^{-1}$  and  $K_{Sdim} = 2.4 \times 10^{-5} \text{ m}^2 \text{ s}^{-1}$ . Stern *et al.* (2001) inferred three-dimensional diffusivities using the two-dimensional results; the two-dimensional/three-dimensional conversion factor was deduced from the selected three-dimensional simulations in the regime numerically accessible to the authors at that time.

In figure 3, we plot typical horizontal ( $a, b$ ) and vertical ( $c, d$ ) of temperature ( $a, c$ ) and salinity ( $b, d$ ) for the fully developed equilibrium regime. Temperature and

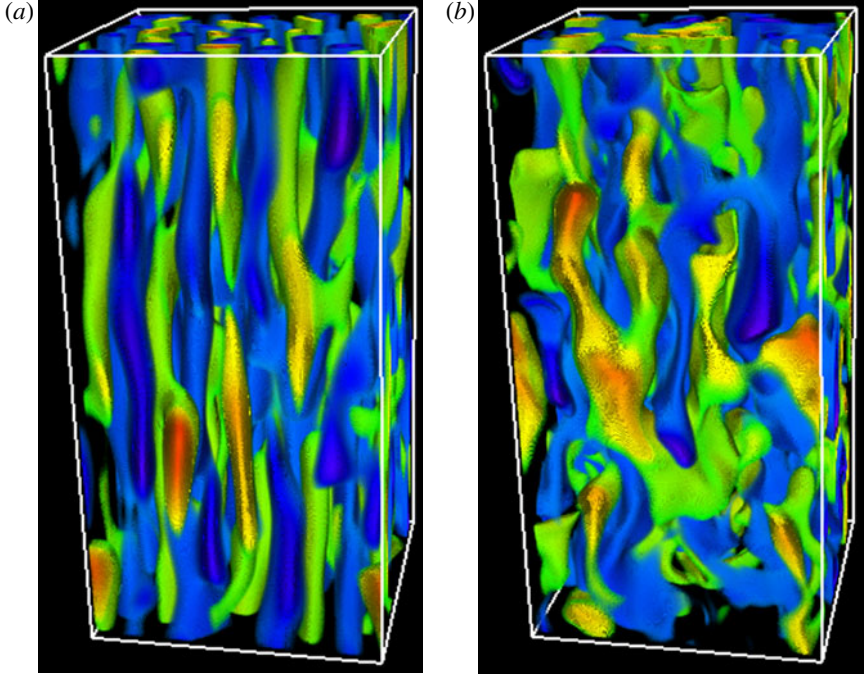


FIGURE 1. Equilibration of salt fingers in the numerical experiment with  $Pr = 7$ ,  $\tau = 0.01$ ,  $R_\rho = 1.9$ . Three-dimensional instantaneous temperature fields are shown for (a) the early stage of linear growth at  $t = 20$  and (b) the fully equilibrated state at  $t = 50$ . Red/green corresponds to high values of  $T$  and low values are shown in blue.

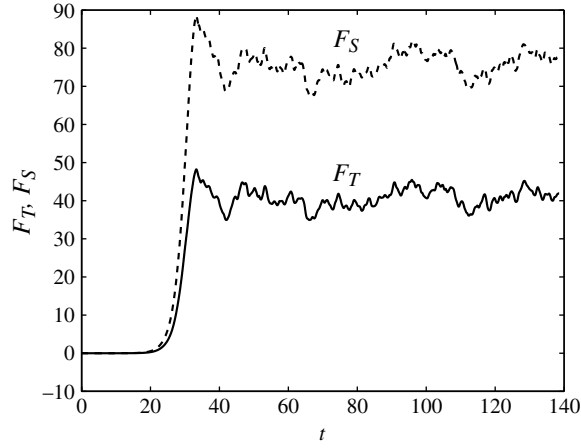


FIGURE 2. Time record of the temperature (solid curve) and salinity (dashed curve) fluxes for the calculation in figure 1.

salinity patterns are correlated and both reveal vertically elongated – but far from uniform – horizontally isotropic salt fingers. Salinity sections are characterized by very fine, relative to temperature, spatial scales, which is a direct consequence of the low diffusivity ratio.

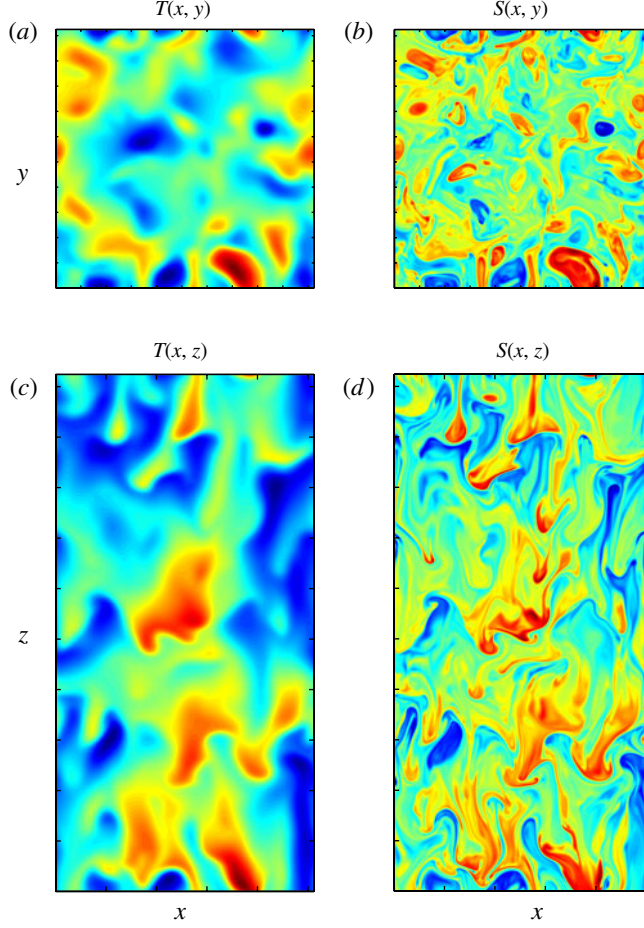


FIGURE 3. Horizontal (*a*, *b*) and vertical (*c*, *d*) sections of temperature (*a*, *c*) and salinity (*b*, *d*) for a typical fully equilibrated state of the calculation in figure 2.

### 3. Theoretical model

Guided by physical reasoning (§ 1) and by DNS (e.g., § 2), we now attempt to predict the equilibrium level of salt fingers from the growth rate balance (1.2). The growth rate equation for the primary salt finger instabilities (Stern 1960) in our non-dimensional units reduces to

$$\begin{aligned} \lambda^3 + [1 + \tau + Pr]k^2\lambda^2 + [(\tau + Pr + \tau Pr)k^4 + Pr(1 - R_\rho^{-1})]\lambda \\ + \tau Prk^6 - Prk^2(R_\rho^{-1} - \tau) = 0, \end{aligned} \quad (3.1)$$

where  $k$  is the horizontal wavenumber of the vertically uniform elevator modes. For our purpose it is not necessary to consider inclined salt fingers since the largest growth rates are attained by the vertically oriented elevator modes (e.g. Baines & Gill 1969). For each  $(R_\rho, Pr, \tau)$ , we compute the largest growth rate  $\lambda_1$  by maximizing the solutions of (3.1) with respect to  $k$  as in Schmitt (1979, 1983). Thus,  $\lambda_1$  is uniquely determined by the governing parameters:

$$\lambda_1 = \lambda_1(R_\rho, Pr, \tau). \quad (3.2)$$

While the maximal growth rates of primary instabilities are identical in two ( $x, z$ ) and three ( $x, y, z$ ) dimensions, the secondary instabilities differ substantially. Therefore, the algorithms for computing  $\lambda_2$  in two and three dimensions will be discussed separately.

### 3.1. Two-dimensional formulation

In two dimensions, the governing equations are conveniently written in terms of the streamfunction  $\psi$ , such that  $(u, w) = (-\partial\psi/\partial z, \partial\psi/\partial x)$ , resulting in

$$\left. \begin{aligned} \frac{\partial T}{\partial t} + J(\psi, T) + \frac{\partial \psi}{\partial x} &= \nabla^2 T, \\ \frac{\partial S}{\partial t} + J(\psi, S) + \frac{1}{R_p} \frac{\partial \psi}{\partial x} &= \tau \nabla^2 S, \\ \frac{\partial}{\partial t} \nabla^2 \psi + J(\psi, \nabla^2 \psi) &= Pr \left[ \frac{\partial}{\partial x} (T - S) + \nabla^4 \psi \right]. \end{aligned} \right\} \quad (3.3)$$

Our next step is to use (3.3) to examine the stability of the basic state representing the elevator modes:

$$\left. \begin{aligned} \bar{T} &= A_T \sin(kx), \\ \bar{S} &= A_S \sin(kx), \\ \bar{\psi} &= A_\psi \cos(kx). \end{aligned} \right\} \quad (3.4)$$

It should be mentioned that the secondary stability problem can be formulated in different ways. Holyer (1984) has chosen the wavenumber  $k$  in (3.4) to correspond to the solution with zero primary growth rate ( $k_0$ ). This restriction defines a well-posed stability problem with the regular basic steady state. The main reason to question this formulation is the following. It is apparent from DNS (Stern *et al.* 2001; Traxler *et al.* 2011) and even indicated by some oceanographic field measurements (Gargett & Schmitt 1982) that the horizontal wavenumber of dominant fully developed salt fingers is more accurately approximated by  $k_{max}$ , the wavenumber corresponding to the maximum growth rate, than by  $k_0$ . Use of  $k = k_{max}$  in (3.4), however, results in the time-dependent basic state, and therefore the conventional methods of stability analysis cannot be applied directly. This problem is not uncommon and not insurmountable. Notable examples of analysing such flows come from studies based on the Kolmogorov model – the sinusoidal parallel flow in viscous fluid (Sivashinsky 1985; Manfroi & Young 1999, 2002; Balmforth & Young 2002, 2005). Since the unforced viscous parallel flow would inevitably decay, the Kolmogorov model circumvents this problem by introducing artificial forcing in the momentum equation that maintains the steady state. Variations on the same principle, often referred to as the quasi steady state approximation or a ‘frozen flow’ method, have been successfully applied to numerous stability problems (e.g. Lick 1964; Robinson 1976) including salt fingers (Kimura & Smyth 2011).

A choice has to be made at this point between the approach of a purist, insisting on formal mathematical consistency, and that of a practically oriented researcher, more concerned by the consistency with patterns realized in nature. We have examined both models,  $k = k_0$  and  $k = k_{max}$ , and the results are qualitatively similar. The prediction of the  $k = k_{max}$  model is closer to the corresponding DNS, and therefore we limit the following discussion to the configuration based on the fastest-growing solution. We also note in passing that the flux ratio of heat and salt ( $\gamma = \alpha F_{Tdim}/\beta F_{Sdim} = F_T/F_S$ ) – an important characteristic of salt fingering that will

be discussed later on – is much better represented by the fastest-growing finger models (e.g. Schmitt 1979) than by marginally stable modes ( $k = k_0$ ).

Assuming that in the regime close to equilibrium the amplitude (3.4) is maintained at a quasi-steady level, we separate the solution into the dominant basic state and small perturbation:

$$(T, S, \psi) = (\bar{T}, \bar{S}, \bar{\psi}) + (T', S', \psi'). \quad (3.5)$$

Equation (3.3) is linearized as follows:

$$\left. \begin{aligned} \frac{\partial T'}{\partial t} - A_\psi k \sin(kx) \frac{\partial T'}{\partial z} - A_T k \cos(kx) \frac{\partial \psi'}{\partial z} + \frac{\partial \psi'}{\partial x} &= \nabla^2 T', \\ \frac{\partial S'}{\partial t} - A_\psi k \sin(kx) \frac{\partial S'}{\partial z} - A_S k \cos(kx) \frac{\partial \psi'}{\partial z} + \frac{1}{R_\rho} \frac{\partial \psi'}{\partial x} &= \tau \nabla^2 S', \\ \frac{\partial}{\partial t} \nabla^2 \psi' - A_\psi k \sin(kx) \frac{\partial \nabla^2 \psi'}{\partial z} - A_\psi k^3 \sin(kx) \frac{\partial \psi'}{\partial z} &= Pr \left[ \frac{\partial}{\partial x} (T' - S') + \nabla^4 \psi' \right]. \end{aligned} \right\} \quad (3.6)$$

To examine the stability properties of the linear system (3.6), we use the Floquet technique in which the perturbation is sought in the following form:

$$\begin{pmatrix} T' \\ S' \\ \psi' \end{pmatrix} = \exp(i f k x + i m z + \lambda t) \sum_{n=-N}^N \begin{pmatrix} T_n \\ S_n \\ \psi_n \end{pmatrix} \exp(inkx), \quad (3.7)$$

where  $\lambda$  is the growth rate,  $m$  is the vertical wavenumber, and  $f$  is the Floquet coefficient, which controls the fundamental wavelength in  $x$ . Substituting (3.7) into the linear system (3.6) and collecting the individual Fourier components allows us to express the governing equations in the matrix form

$$\lambda \xi = \mathbf{A} \xi, \quad (3.8)$$

where

$$\xi = (T_{-N}, S_{-N}, \psi_{-N}, T_{-N+1}, S_{-N+1}, \psi_{-N+1}, \dots, T_N, S_N, \psi_N), \quad (3.9)$$

and  $\mathbf{A}$  is the square matrix whose elements are functions of  $(k, m, f, R_\rho, Pr, \tau, N, A_T, A_S, A_\psi)$ .

The growth rates of the normal modes of the linear system (3.6) correspond to the eigenvalues of  $\mathbf{A}$ . For each set of governing parameters, we determine the eigenvalue with the maximum real part, which represents the fastest-growing mode. The value of this growth rate is then maximized with respect to  $m$  and  $f$ . Note that the symmetry and periodicity properties of our system are such that the Floquet coefficient  $f$  needs to be varied only within the range  $0 \leq f \leq 0.5$ .

The coefficients  $(A_T, A_S, A_\psi)$  of the normal mode (3.4) are connected, for  $k = k_{max}$ , by the following relations:

$$\left. \begin{aligned} A_T(\lambda_1 + k_{max}^2) &= k_{max} A_\psi, \\ A_S(\lambda_1 + \tau k_{max}^2) &= \frac{k_{max}}{R_\rho} A_\psi, \end{aligned} \right\} \quad (3.10)$$

and therefore the amplitude vector  $(A_T, A_S, A_\psi)$  can be immediately determined from any component – for instance from the temperature amplitude  $A_T$ . As described below, the solution rapidly converges with increasing resolution ( $N \rightarrow \infty$ ). Thus, the

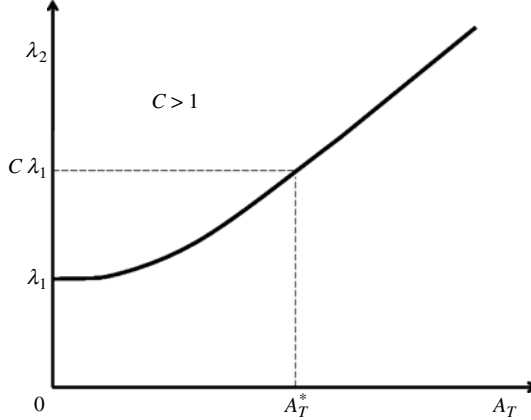


FIGURE 4. Illustration of the algorithm for predicting the equilibrium amplitude of salt fingers. The growth rate of the secondary instability  $\lambda_2$  monotonically increases with the amplitude of salt fingers  $A_T$ . We hypothesize that the equilibrium  $A_T^*$  is reached when  $\lambda_2 = C\lambda_1$ .

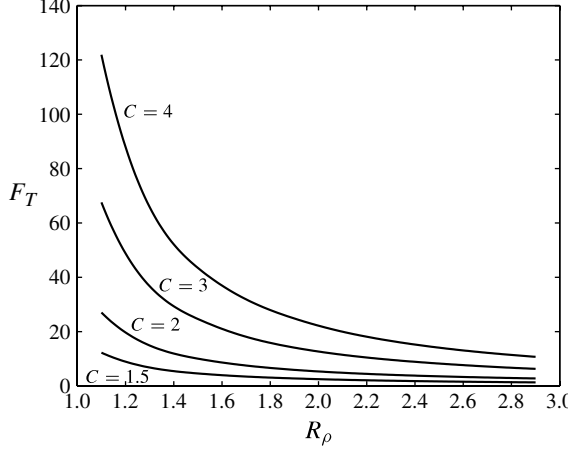
fastest-growing secondary instability is determined by four parameters:

$$\lambda_2 = \lambda_2(R_\rho, Pr, \tau, A_T). \quad (3.11)$$

Our next step is to solve the growth rate balance (1.2). For each set of governing parameters  $(R_\rho, Pr, \tau)$ , we determine the primary growth rate  $\lambda_1$  using (3.1). Suppose now that the value of  $C$  in (1.2) is known. Then, by varying the amplitude of the normal mode  $A_T$ , we can readjust (3.11) until the growth rate balance is satisfied. The dependence  $\lambda_2(A_T)$  takes the form of a monotonically increasing, nearly linear relation. For  $A_T = 0$ , the secondary instability problem becomes identical to that of primary instability and therefore  $\lambda_2 = \lambda_1$ . A corollary of this observation is that solutions of (1.2) exist only for  $C > 1$ , as indicated by the schematic in figure 4. An iterative procedure for solving the growth rate balance (1.2) was coded in Maple and it typically required 7–8 iterations for the model to converge, within a negligible relative error of  $10^{-5}$ , to the sought-after solution  $A_T = A_T^*$ . The vertical fluxes are then reconstructed using (3.4) and (3.10) as follows:

$$\left. \begin{aligned} F_T &= \overline{wT} = \frac{1}{2} A_T^2 (\lambda_1 + k_{max}^2), \\ F_S &= \overline{wS} = \frac{1}{2R_\rho} A_T^2 \frac{(\lambda_1 + k_{max}^2)^2}{(\lambda_1 + \tau k_{max}^2)}. \end{aligned} \right\} \quad (3.12)$$

In figure 5, the predicted heat fluxes are plotted as a function of density ratio for ( $Pr = 7, \tau = 0.01$ ) and various values of  $C$ . Fluxes increase with  $C$  and rapidly reduce with  $R_\rho$ . The calculations in figure 5 were performed for  $N = 32$ . However, the specific number of Fourier harmonics involved in the Floquet calculation is not particularly important. The rapid convergence of the solution with increasing  $N$  is indicated in table 1. The very crude truncation with  $N = 2$  results in 19 % error, whereas the  $N = 4$  error is less than 2 %.

FIGURE 5. Heat flux in the theoretical two-dimensional model for various values of  $C$ .

$N$	$F_T$	$F_S$	$\text{err} = (F_T - F_T _{N=32}/F_T _{N=32})$
2	29.553 87	50.239 65	0.1899
4	25.286 58	42.985 54	0.0181
8	24.839 62	42.225 73	0.0001
16	24.836 68	42.220 74	$\text{err} < 10^{-5}$
32	24.836 68	42.220 74	NA

TABLE 1. Convergence of the Floquet-based algorithm in a two-dimensional calculation for  $(R_\rho, Pr, \tau) = (1.9, 7, 0.01)$ . As the number  $N$  of spectral harmonics increases, the heat flux  $F_T$  rapidly approaches its limiting ( $N \rightarrow \infty$ ) value.

### 3.2. Three-dimensional formulation

Numerical simulations (e.g. Stern *et al.* 2001) reveal significant differences, in magnitude and dynamics, between two-dimensional and three-dimensional salt fingers. Three-dimensional fluxes are systematically higher, by a factor of 2–3, than their two-dimensional counterparts. In this section, we attempt to extend the growth rate balance theory to three dimensions. In addition to the natural interest in three-dimensional dynamics – after all, we live in a three-dimensional world – we are also motivated by the expectation that the results will help to rationalize the difference in the intensity of salt fingers in two and three dimensions. Since the following theory is analogous to the two-dimensional case (§ 3.2), it is presented in abbreviated form.

The essential difference between two-dimensional and three-dimensional dynamics stems from the more complicated structure of the salt finger elevator modes in three dimensions:

$$\left. \begin{aligned} \bar{T} &= A_T \exp(\lambda_1 t) \phi(x, y), \\ \bar{S} &= A_S \exp(\lambda_1 t) \phi(x, y), \\ \bar{w} &= A_W \exp(\lambda_1 t) \phi(x, y), \end{aligned} \right\} \quad (3.13)$$

where the horizontal planform function  $\phi$  satisfies the Helmholtz equation  $\nabla_H^2 \phi + k^2 \phi = 0$ . In three dimensions, identical growth rates can be attained by various

horizontal planforms. For instance, even if we limit our analysis to rectangular planforms

$$\phi = \cos(k_x x) \cos(k_y y), \quad (3.14)$$

all possible configurations with

$$k_x^2 + k_y^2 = k_{max}^2 \quad (3.15)$$

yield the maximum growth rates ( $\lambda_1$ ) and therefore are *a priori* equivalent. The degeneracy of linear theory with respect to the planform selection is well known and can be resolved by invoking fundamentally nonlinear considerations. Proctor & Holyer (1986) and Radko & Stern (2000) examined the problem for a ‘bounded’ configuration, in which the finger layer was limited by rigid horizontal surfaces – the setup analogous to the classical Rayleigh convection problem. The former (latter) study suggested the tendency of the planform to evolve spontaneously to two-dimensional rolls (square cells). For the unbounded regime, some guidance regarding the planform selection was provided by diagnostics of numerical simulations in Radko & Stern (1999), which indicate that the preferred planform is neither square nor a roll, but rather some combination thereof, perhaps best described by the planform function of the type

$$\phi = \cos(k_{max}x) + \frac{1}{2} \cos(k_{max}y), \quad (3.16)$$

which was used in our calculations. It should be mentioned, however, that for our purpose – determination of the equilibrium transport characteristics – the planform choice turns out not to be particularly significant, with the square cell model performing only slightly worse than (3.16).

The calculation of secondary growth rates for the salt fingers with  $(x, y)$ -dependent planform proceeds, as previously, by the method based on Floquet theory. The governing equations (2.1) are linearized with respect to the basic state (3.13), which is assumed to be quasi-steady, and the solution is sought in the following form:

$$\begin{pmatrix} T' \\ S' \\ u' \\ v' \\ w' \\ p' \end{pmatrix} = \exp(i f_x kx + i f_y ky + imz + \lambda t) \sum_{n_x=-N}^N \sum_{n_y=-N}^N \begin{pmatrix} T_{n_x, n_y} \\ S_{n_x, n_y} \\ u_{n_x, n_y} \\ v_{n_x, n_y} \\ w_{n_x, n_y} \\ p_{n_x, n_y} \end{pmatrix} \exp(in_x kx + in_y ky), \quad (3.17)$$

where  $(f_x, f_y)$  are the Floquet factors in  $x$  and  $y$ . Substituting (3.17) in the linearized governing equations and collecting the individual Fourier components reduces the stability problem to matrix form (3.8). Maximizing the growth rates with respect to  $(f_x, f_y, m)$ , we predict the largest growth rates of secondary instabilities ( $\lambda_2$ ) as a function of  $(R_\rho, Pr, \tau, A_T)$ . Finally, for any given  $C$ , we search for the amplitude  $A_T = A_T^*$  that satisfies the growth rate balance (1.2). The vertical fluxes are then reconstructed as follows:

$$\left. \begin{aligned} F_T &= \overline{wT} = \frac{5}{8} A_T^2 (\lambda_1 + k_{max}^2), \\ F_S &= \overline{wS} = \frac{5}{8R_\rho} \frac{A_T^2 (\lambda_1 + k_{max}^2)^2}{(\lambda_1 + \tau k_{max}^2)}, \end{aligned} \right\} \quad (3.18)$$

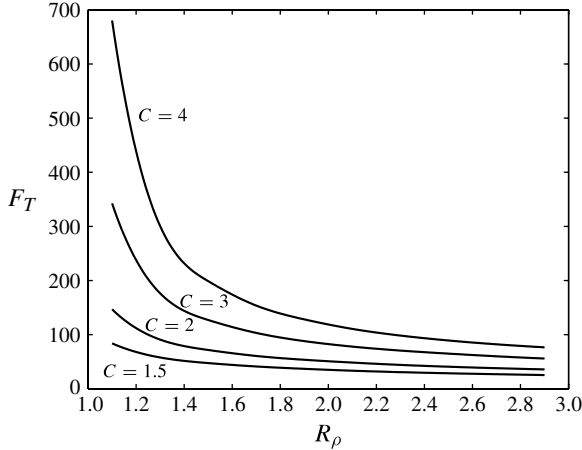


FIGURE 6. Heat flux in the theoretical three-dimensional model for various values of  $C$ .

and  $F_T$  is plotted in figure 6 as a function of density ratio for various values of  $C$ . While the patterns of three-dimensional (figure 6) and two-dimensional (figure 5) fluxes are qualitatively similar – in both cases fluxes rapidly reduce with  $R_\rho$  and increase with  $C$  – they differ in details. In particular, three-dimensional fluxes are consistently higher. This is a direct consequence of the fact that the two-dimensional basic state (3.4) is more unstable than its three-dimensional counterpart (3.13), (3.16). Thus, the amplitude of salt fingers has to be significantly higher in three dimensions to produce secondary instabilities of the same strength as in two dimensions, which rationalizes the behaviour noticed in the numerical simulations of Stern *et al.* (2001).

#### 4. Calibrating the theory: heat–salt experiments

A limitation of the theoretical model in §3 is related to its inability to determine the constant  $C$  internally. Our theory assumes that  $C$  is comparable to unity but does not provide an exact value. In order to calibrate  $C$ , we now turn to DNS. For the heat/salt case ( $Pr = 7, \tau = 0.01$ ) discussed in this section, the analysis is based on 10 two-dimensional simulations and 10 three-dimensional simulations made for  $R_\rho = 1.1, 1.3, \dots, 2.9$ .

Figure 7 presents fluxes from a series of two-dimensional calculations, plotted along with the theoretical prediction from the foregoing growth rate balance theory (§3) with  $C = 4.3$ . In all simulations we used  $(N_x, N_z) = (256, 512)$  grid points and the size of the computational domain  $(L_x, L_z) = (38.2, 76.3)$  equivalent to  $5 \times 10$  linearly fastest-growing finger wavelengths ( $d$ ). The variation of heat (figure 7a) and salt (figure 7b) fluxes with density ratio follows the theoretical pattern very closely. The ability of our model, containing only one adjustable parameter, to capture details of the numerical simulations to such an extent lends credence to the proposed condition (1.2) as the most relevant physical factor constraining growth of salt fingers.

Figure 8 presents the corresponding three-dimensional calculations. The resolution of three-dimensional DNS matched the two-dimensional runs: a  $(N_x, N_y, N_z) = (256, 256, 512)$  mesh was used to resolve  $5 \times 5 \times 10$  fastest-growing finger wavelengths. The theoretical calculation for  $C = 2.7$  is superimposed on the numerical data, revealing their mutual consistency: our theory predicts the right order of magnitude and the pattern of fluxes as a function of  $R_\rho$ . The relevant value of the adjustable

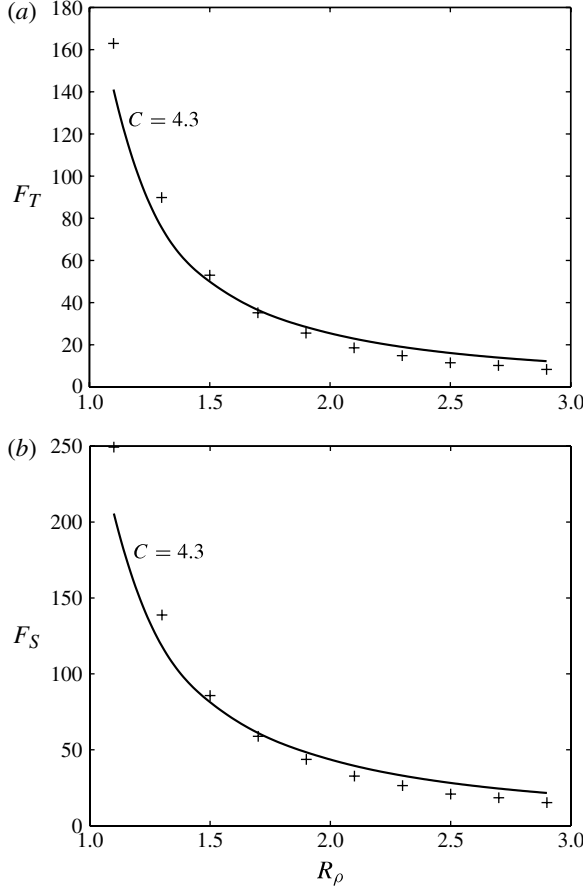


FIGURE 7. Comparison of the theoretical two-dimensional model for  $C = 4.3$  (solid curve) with DNS (plus signs). Heat and salt fluxes are shown in (a) and (b) respectively.

coefficient  $C = 2.7$  in three dimensions is comparable to – but differs from – the two-dimensional value of  $C = 4.3$ . The difference can be readily attributed to distinct equilibrium dynamics of three-dimensional and two-dimensional salt fingers in the unbounded model (Radko & Stern 1999).

While development of explicit parametrizations of double-diffusion for large-scale ocean modelling is outside of our immediate goal, it could prove beneficial for more applied studies to note that the numerical data in figure 8 can be accurately approximated by the following algebraic expressions:

$$\left. \begin{aligned} F_S &= \frac{a_S}{\sqrt{R_\rho - 1}} + b_S, & (a_S, b_S) &= (135.7, -62.75), \\ \gamma &= a_\gamma \exp(-b_\gamma R_\rho) + c_\gamma, & (a_\gamma, b_\gamma, c_\gamma) &= (2.709, 2.513, 0.5128), \\ F_T &= \gamma F_S, \end{aligned} \right\} \quad (4.1)$$

which are indicated in figure 8 by dashed curves. The structure of the expression for  $F_S(R_\rho)$  is suggested by theoretical arguments in Radko (2008), whereas the expression for the flux ratio  $\gamma(R_\rho)$  represents a purely empirical exponential fit to the numerical data.

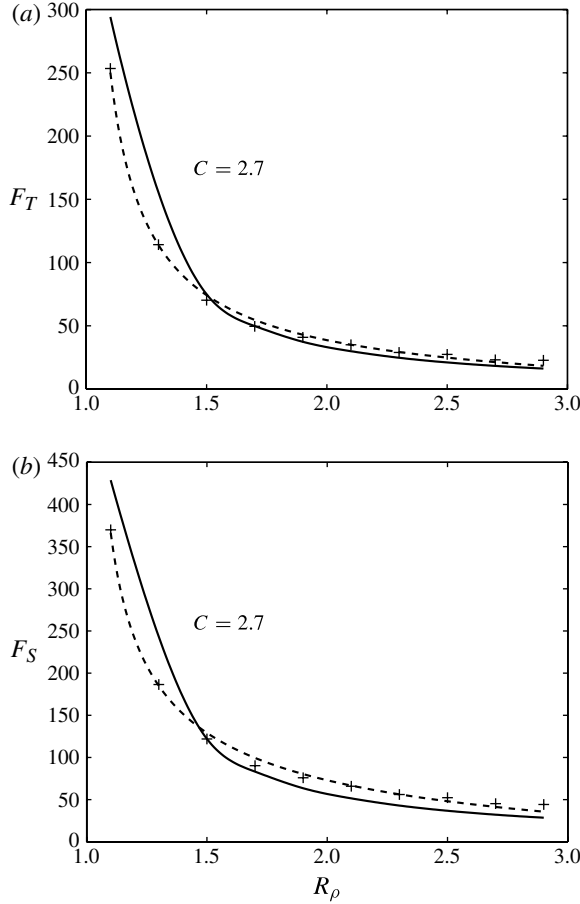


FIGURE 8. The same as in figure 7 but for the three-dimensional model with  $C = 2.7$ . Also plotted are the empirical expressions of fluxes in (4.1), indicated by the dashed curves.

In figure 9, we plot the theoretical flux ratio ( $\gamma = F_T/F_S$ ), which is based on the prediction of the linear fastest-growing finger model (Schmitt 1979), along with the DNS values and their numerical fit in (4.1). While the linear model systematically overestimates the numerical flux ratios by approximately 10%, it captures the general pattern of the  $\gamma(R_\rho)$  relationship. It is important to emphasize that in both theory and simulations the flux ratio decreases with increasing density ratio in the oceanographically relevant range ( $1 < R_\rho < 3$ ). The latter property has been implicated (Radko 2003, 2005; Stellmach *et al.* 2011) in the spontaneous formation of the step-like patterns in vertical temperature and salinity profiles known as thermohaline staircases – perhaps the most dramatic consequence of active double-diffusion in the ocean.

## 5. Generalizations

In this section, we go beyond the oceanographically motivated heat–salt ( $Pr, \tau = (7, 0.01)$ ) case and test the generality of our conclusions by exploring a broader parameter range. The discussion is based on the comparison of four representative

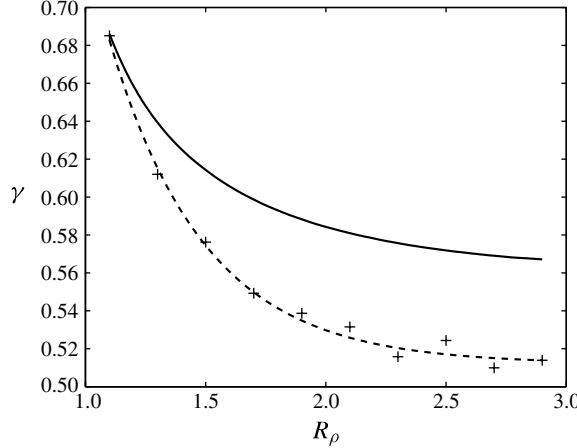


FIGURE 9. Flux ratio as a function of density ratio. DNS results are indicated by plus signs and the solid curve represents prediction of the linear fastest-growing finger model. The empirical expression for the flux ratio in (4.1) is shown by the dashed curve.

series of three-dimensional numerical experiments with corresponding theoretical results:

- Case 1: low Prandtl number ( $Pr, \tau = (0.1, 0.01)$ ).
- Case 2: high Prandtl number ( $Pr, \tau = (100, 0.01)$ ).
- Case 3: high diffusivity ratio ( $Pr, \tau = (7, 0.1)$ ).
- Case 4: sugar–salt experiment ( $Pr, \tau = (1000, 1/3)$ ).

Direct numerical simulations for more extreme parameter values ( $Pr \rightarrow \infty, Pr \rightarrow 0, \tau \rightarrow 0$ ) become computationally prohibitive in three dimensions, and therefore our selection reflects a substantial fraction of the numerically accessible range. In all cases, we performed a series of calculations with  $R_\rho = 1.1, 1.3, \dots, 2.9$  in computational domains corresponding to  $5 \times 5 \times 10$  fastest-growing finger wavelengths, recording the average equilibrium fluxes. Comparing case 1 with our baseline heat–salt configuration allows us to examine specifics of the low-Prandtl-number regime, which is relevant for astrophysical applications. Likewise, differences between case 2 and heat–salt provide a glimpse into the large-Prandtl-number regime, exemplified by double-diffusion in magma chambers. Case 3 differs from the heat–salt calculation by diffusivity ratio, which also varies dramatically between various applications – from  $\tau = 0.8$  for heat/humidity in the atmosphere to  $\tau \sim 10^{-6}$  in stellar interiors. Finally, case 4 represents sugar–salt experiments, which are commonly conducted in laboratory studies because of the relative simplicity of the experimental setup (Stern & Turner 1969; Lambert & Demenkov 1972; Griffiths & Ruddick 1980; Krishnamurti 2003, 2009).

Results are summarized in figure 10, where we plot the equilibrium fluxes of  $T$  and  $S$  (not necessarily representing temperature and salinity) as a function of density ratio. Calculations indicate that fluxes are most strongly affected by variation in the density ratio: as  $R_\rho$  increases from 1.1 to 2.9, fluxes reduce by at least an order of magnitude in all cases considered in this study. Our limited numerical exploration of the effects of the molecular parameters suggests that, for any given  $R_\rho$ , fluxes increase with Prandtl number ( $Pr$ ) and mildly decrease with the diffusivity ratio ( $\tau$ ); see table 2, which lists  $T$ – $S$  fluxes for  $R_\rho = 1.9$ . These dependences are

	$Pr$	$\tau$	$F_T$	$F_S$	$A$
Heat–salt	7	0.01	40.876	75.879	10.56
Case 1	0.1	0.01	1.9140	4.6501	55.86
Case 2	100	0.01	220.185	364.844	7.234
Case 3	7	0.1	39.342	60.260	6.309
Case 4	1000	0.333	959.53	1123.3	0.346

TABLE 2. Dependence of the equilibrium  $T$ – $S$  fluxes on the molecular characteristics ( $Pr$ ,  $\tau$ ) in three-dimensional simulations with  $R_\rho = 1.9$ .

consistent with the prediction based on the growth rate balance model, which is also indicated in figure 10. The relevant values of the adjustable coefficient  $C$  vary only weakly between the various cases considered in this study. The lowest value of  $C = 1.6$  (obtained for case 1) is not too different from the largest value of  $C = 2.7$  (heat–salt case), considering the range of governing parameters and fluxes. Overall, numerical evidence in this study supports the growth rate balance theory as a conceptual model of the equilibrium salt fingering, capable of predicting the equilibrium temperature/salinity transports within a factor of two.

The least accurate prediction was obtained for the sugar–salt configuration (figure 10g, h). Both the theoretical model and DNS exhibit complicated non-monotonic dependence on density ratio that do not match well in detail. The disagreement can be rationalized by noting that the sugar–salt parameters correspond to a special regime in which diffusivities of the density components are comparable. In most other applications,  $\tau \ll 1$  and the system is fully turbulent for the order-one values of  $R_\rho$ . As a result, flux dependences take the form of monotonic power-law relations for all density ratios considered in this study. The situation becomes different for the sugar–salt experiment in which  $\tau = 1/3$ . In this case, the system transitions from a laminar weakly nonlinear regime when the density ratio is close to  $\tau^{-1}$  to a fully turbulent state for  $R_\rho$  closer to unity. As a result, the pattern of fluxes and the dynamics of equilibration exhibit very different behaviour at lower/higher density ratios. Equilibrium fluxes in the sugar–salt case are also sensitive to the assumed horizontal planform of the primary salt fingers. In figure 10(g, h) we plot the theoretical prediction based on the square planform (3.14) along with the prediction based on the planform given by (3.16). The two versions differ in detail but are qualitatively consistent. Even in the sugar–salt case, our theory predicts the right order of magnitude for fluxes and their overall decreasing dependence on density ratio for  $C = 2.5$ .

In table 2, we present the Stern numbers (1.1) realized in various experiments. Even for the fixed density ratio of  $R_\rho = 1.9$ ,  $A$  varies by more than two orders of magnitude – from the highest value of  $A = 55.86$  in case 1 to the lowest  $A = 0.346$  in the sugar–salt experiment. Note that the Stern number for the numerical sugar–salt experiment significantly exceeds values obtained in some of the laboratory experiments, for instance  $A \sim 2 \times 10^{-3}$  in Lambert & Demenkov (1972). Our calculation is more consistent with the measurements of Krishnamurti (2003), who obtained Stern numbers in the range  $A = 0.2$ – $0.4$ . One of the possible reasons for the variation in the laboratory estimates is related to the difference in the experimental setup. Lambert & Demenkov (1972) studied salt fingers in a thin interface sandwiched between well-mixed reservoirs, whereas Krishnamurti (2003) used deep gradients

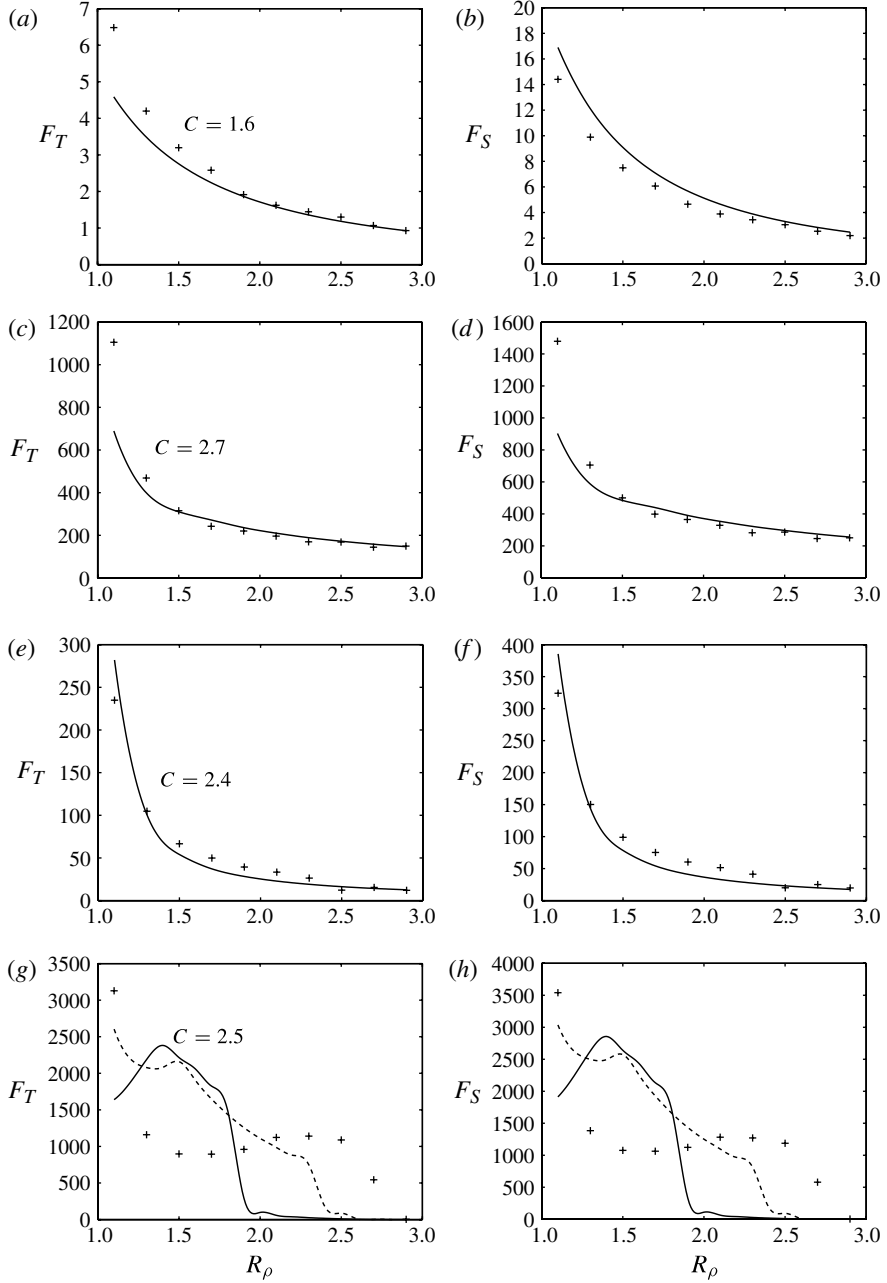


FIGURE 10.  $T$ -flux (*a, c, e, g*) and  $S$ -flux (*b, d, f, h*) as a function of density ratio for: (*a, b*)  $Pr = 0.1$ ,  $\tau = 0.01$  (case 1); (*c, d*)  $Pr = 100$ ,  $\tau = 0.01$  (case 2); (*e, f*)  $Pr = 7$ ,  $\tau = 0.1$  (case 3) and (*g, h*)  $Pr = 1000$ ,  $\tau = 1/3$  (case 4). Solid curves indicate prediction of the theoretical three-dimensional model and DNS results are represented by plus signs. The dashed curve in (*g, h*) corresponds to the theoretical prediction based on the square salt finger planform.

of temperature and salinity that were set up initially. Our numerical configuration represents a much closer analogue of the latter, effectively unbounded system.

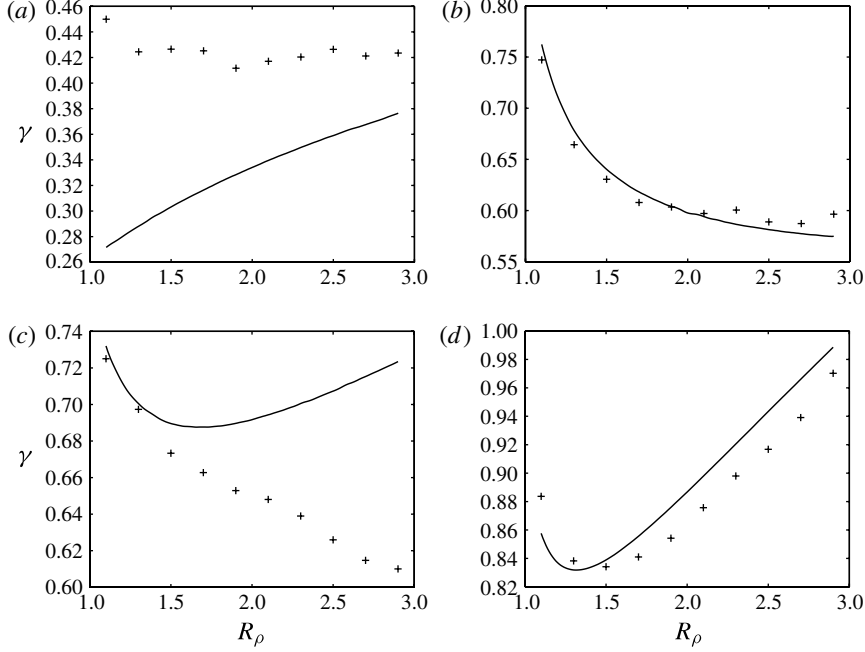


FIGURE 11. Flux ratio as a function of density ratio for (a)  $Pr = 0.1, \tau = 0.01$  (case 1); (b)  $Pr = 100, \tau = 0.01$  (case 2); (c)  $Pr = 7, \tau = 0.1$  (case 3) and (d)  $Pr = 1000, \tau = 1/3$  (case 4). DNS results are indicated by plus signs and the solid curve represents prediction of the linear fastest-growing finger model.

For completeness, we also show (figure 11) the flux ratios from DNS plotted as a function of density ratio, along with the estimates based on the linear fastest-growing finger model (Schmitt 1979). In all cases considered, the linear model performs reasonably well in terms of predicting the typical values of the flux ratio, although its performance depends strongly on the molecular parameters. The closest agreement was observed for the high Prandtl number calculations (cases 2 and 4). This can be attributed to a more vertical orientation of salt fingers in high-Prandtl-number media, apparent from visual inspection of the  $T$ - $S$  fields. The vertical orientation makes the salt finger pattern and dynamics more consistent with the elevator modes considered by Schmitt (1979, 1983), and therefore his model naturally predicts flux ratios more accurately for high  $Pr$ . Note also that in all simulations with moderate and high  $Pr$ , both DNS and linear model predict a decreasing  $\gamma(R_\rho)$  relation in some regions of the parameter space. This signifies the propensity to form thermohaline staircases when much longer wavelengths are allowed in the system (Radko 2003, 2005; Stellmach *et al.* 2011). For the relatively low Prandtl number (case 1) relevant to astrophysical applications, linear theory suggests an increasing  $\gamma(R_\rho)$  relation, whereas direct numerical simulations yield approximately uniform flux ratio, indicating that spontaneous formation of staircases is unlikely.

## 6. Discussion

This paper presents a phenomenological model for the vertical transport by salt fingers in unbounded temperature and salinity gradients, which is based on the growth rate balance hypothesis. Theory assumes that statistical equilibrium is reached

when the growth rate of salt fingers becomes comparable to the growth rate of their secondary instabilities. This assumption can be rationalized as follows. If the growth rate of primary salt fingers exceeds that of secondary instabilities, then the primary instabilities are unlikely to be affected by perturbations and continue to grow. If, on the other hand, the secondary instabilities grow much faster than the fingers, they would rapidly disrupt the primary modes, dramatically reducing their amplitude and transport characteristics. Thus, one is led to a conclusion that the approximate balance between the growth rates of primary and secondary instabilities is inevitable for statistical equilibrium and should be satisfied for a wide range of governing parameters.

The typical growth rates of primary instabilities  $\lambda_1$  are estimated from the well-known linear instability theory. In non-dimensional units,  $\lambda_1$  is a function of density ratio, Prandtl number and diffusivity ratio:  $\lambda_1 = \lambda_1(R_\rho, Pr, \tau)$ . The growth rate of secondary instabilities is additionally affected by the amplitude of the primary salt fingers  $\lambda_2 = \lambda_2(R_\rho, Pr, \tau, A_T)$ , and can be evaluated using Floquet theory. The growth rate balance  $\lambda_1 \sim \lambda_2$  thus implicitly determines the equilibrium amplitude of salt fingers ( $A_T$ ). Knowing  $A_T$ , it becomes possible to evaluate mixing characteristics of fully developed double-diffusive convection. The growth rate balance hypothesis is the basis of an efficient algorithm for computing the vertical eddy diffusivities of heat and salt as a function of density ratio ( $R_\rho$ ) and molecular characteristics ( $k_T, k_S, v$ ) developed in this study.

It should be understood that the growth rates, both primary ( $\lambda_1$ ) and secondary ( $\lambda_2$ ), can only be estimated in the order-of-magnitude sense. Calculation of  $\lambda_1$  is made for the fastest-growing salt fingers – the vertically uniform elevator modes – whereas fully developed double-diffusive convection is generally dominated by irregular structures of finite vertical extent. Similar problems arise for secondary instabilities:  $\lambda_2$  is estimated for the steady and vertical background field, neither of which is an exact statement. In view of these difficulties, we can only claim that the growth rates estimated by our theory ( $\lambda_1$  and  $\lambda_2$ ) should be comparable, but not necessarily equal. Thus, we consider a weak form of the growth rate balance in (1.2). The non-dimensional order-one coefficient  $C$  in (1.2) cannot be determined internally on the basis of theory, and therefore it was calibrated using DNS. For each  $(Pr, \tau)$ , theory adequately describes the (rapidly decreasing) dependence of fluxes of diffusing components on density ratio. The calibrated coefficients  $C$  are fairly stable. In all three-dimensional simulations – simulations that cover four orders of magnitude in  $Pr$  and more than an order of magnitude in  $\tau$  – the values of  $C$  are limited to a relatively narrow range  $1.6 < C < 2.7$ .

The consistency of the growth rate balance theory with DNS is encouraging. While the advent of modern high-performance computers has recently made it possible to model double-diffusion in the oceanic (heat–salt) context, other systems remain inaccessible. Astrophysical applications, for instance, are characterized by extremely low values of Prandtl number and diffusivity ratio ( $Pr \sim 10^{-5}$  and  $\tau \sim 10^{-6}$ ), which implies that the dissipation scales of momentum, temperature and salinity are drastically different. The requirement to resolve these distinct scales in DNS presents a formidable challenge – one that will not be met in the foreseeable future. In such situations, greater importance should be ascribed to our theoretical model. The successful testing by DNS in the numerically accessible regimes suggests that the model is likely to perform well in other, more challenging environments, where it can become the only source of quantitative information.

The model and its successful validation bring some insight into the dynamics of equilibration. In particular, it has been reported in several modelling studies (e.g. Stern *et al.* 2001; Traxler *et al.* 2011) that three-dimensional fluxes considerably exceed their two-dimensional counterparts. This observation can be readily rationalized using the growth rate balance (1.2). For the same amplitudes and primary growth rates, the growth rates of secondary instabilities are substantially less in three dimensions than in two. This implies that three-dimensional salt fingers can grow to much larger amplitudes before the onset of equilibration by secondary instabilities, resulting in larger heat/salt fluxes.

Finally, it is important to emphasize the theoretical significance of our model. In its present form, our algorithm still contains some numerical elements, such as the Floquet-based calculation of the secondary growth rates. However, we believe that this study opens opportunities for purely analytical explorations that are focused on the growth rate balance equation (1.2), rather than on the more complicated original Navier–Stokes system. Our optimism is partly based on the pronounced low-order dynamics of our model. The calculations made with highly truncated ( $N = 2$ ) Fourier series in the Floquet calculation differ from the excessively resolved (say,  $N = 32$ ) calculations by less than 20 %. Thus, it is likely that the general character of our solutions would be captured by an analytical low-dimensional model.

The authors thank J. Flanagan, R. Schmitt, W. Smyth and reviewers for helpful comments. Support by the National Science Foundation (grants OCE 0547650, AST 0806431, CBET 0933057 and ANT 0944536) is gratefully acknowledged.

#### REFERENCES

- BAINES, P. G. & GILL, A. E. 1969 On thermohaline convection with linear gradients. *J. Fluid Mech.* **37**, 289–306.
- BALMFORTH, N. J., GHADGE, S. A., KETTAPUN, A. & MANDRE, S. D. 2006 Bounds on double-diffusive convection. *J. Fluid Mech.* **569**, 29–50.
- BALMFORTH, N. J. & YOUNG, Y.-N. 2002 Stratified Kolmogorov flow. *J. Fluid Mech.* **450**, 131–167.
- BALMFORTH, N. J. & YOUNG, Y.-N. 2005 Stratified Kolmogorov flow. Part 2. *J. Fluid Mech.* **528**, 23–42.
- CANUTO, V. M., CHENG, Y. & HOWARD, A. M. 2008 A new model for Double Diffusion + Turbulence. *Geophys. Res. Lett.* **35**, L02613.
- CHARBONNEL, C. & ZAHN, J. 2007 Thermohaline mixing: a physical mechanism governing the photospheric composition of low-mass giants. *Astron. Astrophys.* **467**, L29–L32.
- GARGETT, A. E. & SCHMITT, R. W. 1982 Observations of salt fingers in the central waters of the eastern North Pacific. *J. Geophys. Res.* **87**, 8017–8092.
- GRIFFITHS, R. W. & RUDDICK, B. R. 1980 Accurate fluxes across a salt–sugar finger interface deduced from direct density measurements. *J. Fluid Mech.* **99**, 85–95.
- GUILLOT, T. 1999 Interiors of giant planets inside and outside the solar system. *Science* **286**, 72–77.
- HEBERT, D. 1988 Estimates of salt-finger fluxes. *Deep-Sea Res.* **35**, 1887–1901.
- HOLYER, J. Y. 1984 The stability of long, steady, two-dimensional salt fingers. *J. Fluid Mech.* **147**, 169–185.
- HOWARD, L. N. 1961 Note on a paper of John W. Miles. *J. Fluid. Mech.* **10**, 509–512.
- INOUE, R., KUNZE, E., ST LAURENT, L., SCHMITT, R. W. & TOOLE, J. M. 2008 Evaluating salt fingering theories. *J. Mar. Res.* **66**, 413–440.
- KIMURA, S. & SMYTH, W. D. 2007 Direct numerical simulation of salt sheets and turbulence in a double-diffusive shear layer. *Geophys. Res. Lett.* **34**, L21610.

- KIMURA, S. & SMYTH, W. D. 2011 Secondary instability of salt sheets. *J. Mar. Res.* (submitted).
- KRISHNAMURTI, R. 2003 Double-diffusive transport in laboratory thermohaline staircases. *J. Fluid Mech.* **483**, 287–314.
- KRISHNAMURTI, R. 2009 Heat, salt and momentum transport in a laboratory thermohaline staircase. *J. Fluid Mech.* **638**, 491–506.
- KUNZE, E. 1987 Limits on growing, finite length salt fingers: a Richardson number constraint. *J. Mar. Res.* **45**, 533–556.
- LAMBERT, R. B. & DEMENKOW, J. W. 1972 On the vertical transport due to fingers in double diffusive convection. *J. Fluid Mech.* **54**, 627–640.
- LICK, W. 1964 The instability of a fluid layer with time-dependent heating. *J. Fluid Mech.* **21**, 565–576.
- MANFROI, A. & YOUNG, W. 1999 Slow evolution of zonal jets on the beta plane. *J. Atmos. Sci.* **56**, 784–800.
- MANFROI, A. & YOUNG, W. 2002 Stability of beta-plane Kolmogorov flow. *Physica D* **162**, 208–232.
- MERRYFIELD, W. J. & GRINDER, M. 1999 Salt fingering fluxes from numerical simulations (unpublished manuscript).
- MILES, J. W. 1961 On the stability of heterogeneous shear flows. *J. Fluid. Mech.* **10**, 496–508.
- PROCTOR, M. R. E. & HOLYER, J. Y. 1986 Planform selection in salt fingers. *J. Fluid Mech.* **168**, 241–253.
- RADKO, T. 2003 A mechanism for layer formation in a double-diffusive fluid. *J. Fluid Mech.* **497**, 365–380.
- RADKO, T. 2005 What determines the thickness of layers in a thermohaline staircase? *J. Fluid Mech.* **523**, 79–98.
- RADKO, T. 2008 The double-diffusive modon. *J. Fluid Mech.* **609**, 59–85.
- RADKO, T. 2010 Equilibration of weakly nonlinear salt fingers. *J. Fluid Mech.* **645**, 121–143.
- RADKO, T. & STERN, M. E. 1999 Salt fingers in three dimensions. *J. Mar. Res.* **57**, 471–502.
- RADKO, T. & STERN, M. E. 2000 Finite amplitude salt fingers in a vertically bounded layer. *J. Fluid Mech.* **425**, 133–160.
- RICHARDSON, L. F. 1920 The supply of energy from and to atmospheric eddies. *Proc. R. Soc. A* **97**, 354–373.
- ROBINSON, J. L. 1976 Theoretical analysis of convective instability of a growing horizontal thermal boundary layer. *Phys. Fluids* **19**, 778–791.
- SCHMITT, R. W. 1979 The growth rate of supercritical salt fingers. *Deep-Sea Res.* **26A**, 23–44.
- SCHMITT, R. W. 1983 The characteristics of salt fingers in a variety of fluid systems, including stellar interiors, liquid metals, oceans, and magmas. *Phys. Fluids* **26**, 2373–2377.
- SCHMITT, R. W., LEDWELL, J. R., MONTGOMERY, E. T., POLZIN, K. L. & TOOLE, J. M. 2005 Enhanced diapycnal mixing by salt fingers in the thermocline of the tropical Atlantic. *Science* **308**, 685–688.
- SCHMITT, R. W., PERKINS, H., BOYD, J. D. & STALCUP, M. C. 1987 C-SALT: an investigation of the thermohaline staircase in the western tropical North Atlantic. *Deep-Sea Res.* **34**, 1697–1704.
- SHEN, C. Y. 1995 Equilibrium salt-fingering convection. *Phys. Fluids* **7**, 706–717.
- SIVASHINSKY, G. 1985 Weak turbulence in periodic flows. *Physica D* **17**, 243–255.
- STANCLIFFE, R., GLEBBEEK, E., IZZARD, R. & POLS, O. 2007 Carbon-enhanced metal-poor stars and thermohaline mixing. *Astron. Astrophys.* **464**, L57–L60.
- STELLMACH, S., TRAXLER, A., GARAUD, P., BRUMMELL, N. & RADKO, T. 2011 Dynamics of fingering convection. Part II. The formation of thermohaline staircases. *J. Fluid Mech.* **667**, 554–571.
- STERN, M. E. 1960 The ‘salt-fountain’ and thermohaline convection. *Tellus* **12**, 172–175.
- STERN, M. E. 1969 Collective instability of salt fingers. *J. Fluid Mech.* **35**, 209–218.
- STERN, M. E., RADKO, T. & SIMEONOV, J. 2001 Three-dimensional salt fingers in an unbounded thermocline with application to the central ocean. *J. Mar. Res.* **59**, 355–390.

- STERN, M. E. & SIMEONOV, J. 2004 Amplitude equilibration of sugar–salt fingers. *J. Fluid Mech.* **508**, 265–286.
- STERN, M. E. & SIMEONOV, J. 2005 The secondary instability of salt fingers. *J. Fluid Mech.* **533**, 361–380.
- STERN, M. E. & TURNER, J. S. 1969 Salt fingers and convective layers. *Deep-Sea Res.* **16**, 497–511.
- ST LAURENT, L. & SCHMITT, R. W. 1999 The contribution of salt fingers to vertical mixing in the North Atlantic tracer release experiment. *J. Phys. Oceanogr.* **29**, 1404–1424.
- TAIT, S. & JAUPART, C. 1989 Compositional convection in viscous melts. *Nature* **338**, 571–574.
- TAYLOR, J. R. & VERONIS, G. 1996 Experiments on doubly-diffusive sugar–salt fingers at high stability ratio. *J. Fluid Mech.* **321**, 315–333.
- TRAXLER, A., STELLMACH, S., GARAUD, P., RADKO, T. & BRUMMEL, N. 2011 Dynamics of fingering convection. Part I. Small-scale fluxes and large-scale instabilities. *J. Fluid Mech.* **677**, 530–553.
- VAUCLAIR, S. 2004 Metallic fingers and metallicity excess in exoplanets’ host stars: the accretion hypothesis revisited. *Astrophys. J.* **605**, 874–879.